Silver nanowire-based transparent electrodes for V2O5 thin films with electrochromic properties

Ambreen Khan, Brandon Faceira, Laetitia Bardet, Camilo Sanchez-Velasquez, Suraj S Nayak, Carmen Jiménez, David Muñoz-Rojas, Aline Rougier, Daniel Bellet

Silver Nanowires-based Transparent Electrodes for V_2O_5 Thin Films with Electrochromic Properties

Ambreen Khan[1,2], Brandon Faceira[2], Laetitia Bardet[1], Camilo Sanchez-Velasquez[1], Suraj S. Nayak[2], Carmen Jiménez[1], David Muñoz-Rojas[1], Aline Rougier[2], Daniel Bellet[1]**

[1]Univ. Grenoble Alpes, CNRS, Grenoble INP, LMGP, 38000 Grenoble, France

[2]Univ. Bordeaux, CNRS, Bordeaux INP, ICMCB, UMR 5026, F-33600 Pessac, France

* Correspondence: Daniel.bellet@grenoble-inp.fr; Aline.rougier@icmcb.cnrs.fr (Tel.: D.B +33-456-529-337, A.R +33 -540-006-263)

KEYWORDS:

Metallic nanowires, conformal oxide coating, interfaces, stability, electrochromic oxide

ABSTRACT:

The development of electrochromic systems, known for the modulation of their optical properties under an applied voltage, depends on the replacement of the state-of-the-art ITO (In_2O_3:Sn) transparent electrode (TE) as well as the improvement of the electrochromic films. This study presents an innovative ITO-free electrochromic film architecture utilizing oxide-coated silver nanowire (AgNW) networks as a TE and V_2O_5 as the electrochromic oxide (EC) layer. The TE

was prepared by simple spray deposition of AgNWs that allow tuning different densities of the network and hence resistance and transparency of the film. The oxide coating (SnO_2 or ZnO) on AgNWs was deposited by Atmospheric-Pressure Spatial Atomic Layer Deposition (AP-SALD), an open-air fast and scalable process yielding a highly stable electrode. V_2O_5 thin films were then deposited by radio frequency magnetron sputtering on the AgNW-based TE. Independently of the oxide nature, a 20 nm protective layer thickness was insufficient to prevent the deterioration of the AgNW network during V_2O_5 deposition. On the contrary, V_2O_5 films grown on 30 nm thick ZnO or SnO_2-coated AgNWs were crystallized exhibiting a typical orange color. Electrochromic characterizations demonstrated that only V_2O_5 films deposited on 30 nm thick SnO_2-coated AgNW showed characteristic oxidation-reduction peaks in Li^+-based liquid electrolyte associated with a reversible orange-to-blue color switch for at least 500 cycles. The electrochromic key properties of AgNW/SnO_2 (30 nm)/V_2O_5 films are discussed in terms of structural and morphological changes due to the AgNW network and the nature and thickness of the two protective oxide coatings.

1. INTRODUCTION

The rapid increase in energy demand due to technological advancements, associated as well to population growth, has resulted in a substantial surge in energy consumption within the building sector. The latter accounts for approximately 40% of the world's total energy consumption[1]. The energy utilization in buildings mainly encounters the demand for heating, air conditioning, and lighting. Electrochromic windows constitute a promising solution to reduce the energy demand and energy losses in the building sector compared to conventional windows[2-3]. Electrochromic devices are based on electrochromic materials that reversibly change their color, and hence optical properties (such as transparency and reflection), resulting from a redox reaction when an electrical

potential is applied. Besides buildings, electrochromic devices have gained tremendous interest in other areas like aircraft windows, displays, automobile sunroofs, switchable sunglasses, sensors, and covers for greenhouses[4-5]. An electrochromic device consists of several layers arranged in a specific order. It typically includes an electrochromic layer and a counter electrode separated by an electrolyte that are sandwiched between two transparent conducting layers.

The transparent electrode (TE) often consists of a layer of conductive metal oxide thin films, such as indium or fluorine-doped tin oxide (ITO and FTO)[6]. Currently, ITO is extensively used as a TE, for most optoelectronic devices, owing to its high transparency, electrical conductivity, and chemical stability[7-8]. However, the scarcity of indium, the expensive deposition method, and the brittleness of ITO prompted the research for new flexible, stable, and low-cost transparent conducting materials[9]. Much research efforts have been focused on alternative transparent conducting materials like carbon nanotubes[10-11], graphene[12-13], metallic grids[14], conductive polymers (PEDOT: PSS)[15], metallic layer like silver [16], and metallic nanowires[17-18]. Among these materials, AgNW networks appear as a promising candidate thanks to their high optical transparency, including in the near-infrared (NIR) region, excellent electrical properties, mechanical flexibility, low cost, and scalability [19]. Conversely, ITO is brittle and therefore not suitable for flexible devices and cannot be modulated for NIR region[12]. Besides, the high aspect ratio of the nanowires gives the network rather similar performances than ITO-based electrodes while consuming much less raw material [20]. However, one of the main factors limiting the integration of AgNW networks in industrial devices is their stability issues when subjected to thermal stress, electrical stress, and environmental stress that led to an early failure of the networks[21-23].

Several approaches to improve the stability of AgNWs networks have been reported in the literature[24]. One of them is the deposition of a thin protective oxide layer on top of the AgNW network, using one of the different techniques such as atomic layer deposition (ALD)[25], chemical vapour deposition (CVD)[26], spin coating[27], dip coating[28] or spray coating[29]. In recent study, Hao, T. et al, have reported the utilization of surface-modified AgNW transparent electrode. The enhancement in adhesion of AgNWs on polyethylene terephthalate (PET) substrate was achieved through surface modification using amino silane. Furthermore, the introduction of a titanium dioxide (TiO_2) coating played a pivotal role in augmenting the stability of the AgNW, contributing to the overall robustness of the electrochromic device [30]. It has been reported that graphene oxide (GO) as passivation layer on AgNWs offers enhanced chemical and thermal stability either as layer of reduced GO due to its gas-barrier properties[31], or as a sandwich like structure covering AgNWs on both sides[32]. Song et al., reported that a thin layer of TiO_2 improves the thermal stability without compromising the electrical performance of AgNWs[33]. Similarly, a bilayer of ZnO and Al_2O_3[34], and ZnO/MgO composite[35] have also shown improvement in mechanical bending properties in addition to thermal and electric stability. The incorporation of ZnO-coated AgNWs within the polymer matrix provides several benefits, including enhanced thermal stability and a smooth surface[25]. However, some techniques used to deposit oxides on AgNWs have several disadvantages, including the complexity, vacuum processing and high price that hinder the scalability of process. An alternative low-cost and fast coating method is atmospheric-pressure spatial atomic layer deposition (AP-SALD). Several reports have shown that this technique is capable of producing high-quality conformal films on the AgNWs[36], such as, ZnO[37-38], Al:ZnO[39] and SnO_2[40-41]. The coatings improved the stability of AgNWs since the metal oxide layer hinders the surface diffusion of the Ag atoms from nanowires, and thus maintaining the integrity and

stability of the nanowire morphology. The stability of AgNWs improves as the coating thickness increases. However, there is a linear decrease in optical transparency as the coating thickness increases[34]. Consequently, a careful consideration of the oxide thickness and chemical nature is essential, depending on the targeted applications.

The EC layer comprises an optically active material capable of modulating its optical state in response to applied potential. Serving as both an electronic and ionic conductor, the EC layer undergoes changes in its optical properties through the insertion and de-insertion of ions at a specific applied potential. Electrochromic materials encompass a diverse range, including polymers, viologen-based compounds, prussian blue compounds, and metal oxides[42]. Among the extensively investigated oxide materials, vanadium pentoxide (V_2O_5) exhibits multichromism due to its various oxidation states and corresponding distinct color. V_2O_5 possesses a layered structure with interlayer spacing that facilitates the insertion and de-insertion of lithium ions, thus enabling reversible changes in its optical properties[43-46].

The aim of the present work is to prepare indium-free electrochromic films using stable AgNW network as TE. The AgNW network was deposited by spray-coating on transparent glass substrates. To overcome AgNW instability issues, the networks were coated with a thin conformal protective oxides layer, namely ZnO and SnO_2, using the AP-SALD method. This study employed two different thicknesses (20 nm and 30 nm) for both ZnO and SnO_2 coated on AgNWs. The influence of post deposition treatment and different thicknesses of protective oxides on the properties and stability of AgNW network are discussed. The electrochromic oxide, V_2O_5, was deposited onto both bare and coated AgNWs using the radio frequency magnetron sputtering (RFMS) technique. The electrochromic performance of the resulting films was assessed using cyclic voltammetry (CV) and chronoamperometry (CA) techniques. Additionally, *in situ* optical

transmittance measurements were conducted at a wavelength of 400 nm during chronoamperometry to evaluate the coloration efficiency and switching time of the as-prepared films. Our results show that AgNWs coated with 30 nm of SnO_2 can be used as indium free TE for electrochromic devices.

2. EXPERIMENTAL SECTION

2.1 Materials

Silver nanowires dispersed in isopropanol (23.6 g/L of silver, 70 nm in diameter and 10 µm in length) were purchased from Protavic International and diluted before use. Isopropanol (C_3H_8O, analytical grade), obtained from Aldrich, was used as solvent to dilute the AgNW solutions. Corning® glass was used as substrates, purchased from Delta Technologies, Limited, Loveland, CO, USA. Tin (II) acetylacetonate and diethyl zinc (both from Aldrich), were employed as Sn and Zn precursors for the AP-SALD coating. Pure vanadium metal (99.9 %) was used as vanadium target for the deposition of V_2O_5. LiTFSI-EmimTFSI, Lithium bis(trifluoromethanesulfonyl)imide: 1-Ethyl-3methyl imidazolium bis-(trifluoromethanesulfonyl) imide (1:9 mol%, 99.9 %), from Solvionic, was used as electrolyte. All chemicals used in the study were employed as received without any purification steps.

2.2 Fabrication of the transparent electrodes (TE)

The 25 x 25 mm^2 corning glass substrates were cleaned ultrasonically in ethanol and DI water for 15 min, and then dried with N_2 gas. The diluted AgNW solutions obtained from Protavic were diluted in isopropanol up to a concentration of 0.23 g/L. AgNWs were then spray deposited on the substrates using a commercial airbrush, moving along two perpendicular directions, in a periodic array over the specified area of specimen. The airbrush was connected to an air pump; thus, pressure of the pump and needle position allowed to adjust the flow rate. The deposition was

performed at a flow rate of 1 droplet every 6 s and at a pressure of 1.4 bar. The substrates were placed on a heating plate at 110 °C, which facilitates the evaporation of solvent after each deposition cycle (avoiding the formation of any coffee rings) and leaves behind the nanowires on the substrates. The targeted resistance for each sample was controlled by an *in situ* measurement of the resistance. This was done by using a bare glass with two parallel contacts on opposite sides, thanks to silver paste (L-200N, CDS electronics), connected to a 2-probe multimeter and resistance was measured as the AgNW networks form and get denser. All the AgNWs were then thermally annealed at 200 °C for 1 h.

The AgNW networks were coated with very thin and conformal layers of protective oxides, either ZnO or SnO_2, using AP-SALD at 200 °C in air. The utilized SALD employs a proximity method relying on a gas manifold. The detailed explanation of the experimental procedure and deposition parameters used can be found in the following articles[36, 40, 47]. The distance between the substrate and the AP-SALD head was set to 150 µm. The deposition rate was 0.26 nm/s and 0.02 nm/s for ZnO and SnO_2, respectively. The thickness of both protective oxides on AgNWs was around 20 or 30 nm, depending on the chosen number of SALD cycles, as revealed by transmission electron microscopy measurements.

2.3 Deposition of the V_2O_5 EC layer

The electrochromic V_2O_5 layer was deposited on the AgNW based TE through RFMS in a PLASSYS MP700S apparatus. The sputtering target was 3 mm thick and 75 mm in diameter vanadium metal plate (99.9 % purity purchased from Neyco), at a base pressure of 3.10^{-7} mbar. The vanadium target was first pre-sputtered under an argon atmosphere at 200 W, 5 Pa for a duration of 30 min. Afterward, plasma stabilization was performed with the shutter closed for 20 min at deposition conditions that correspond to 200 W, total pressure of 2 Pa with flow rate of 45

sccm Ar and 5 sccm O_2. The shutter was then opened to allow deposition on the substrate for 80 min without intentional heating of the substrate. However, the temperature evolves during the process as heat is generated through the plasma. The temperature evolution during the sputtering was monitored every 10 min thanks to the thermocouple located 10 mm away from the substrate holder. The temperature increased up to 210 °C until the end of deposition shown in Figure S1. For the sake of comparison, V_2O_5 was deposited on bare AgNW, ZnO-coated and SnO_2-coated AgNW networks.

2.4 Characterization methods

The optical characteristics of the TE were analyzed using a Perkin Elmer Lambda 950 UV-Visible-NIR spectrophotometer. For each sample the total and diffuse transmittance were measured using an integrating sphere, in the wavelength range 250 to 2500 nm. The electrical resistance was measured by a 4-point probe method (LUCAS LABS SP4) as an average of 5 measurements taken at different specimen locations and 2-probe multimeter using silver paste on two parallel edges of the samples. The morphology of the films was investigated through a field-emission gun scanning electron microscope (FEG-SEM Zeiss Gemini 300, Carl Zeiss Microscopy GmbH, Oberkochen, Germany), equipped with EDS (energy dispersive spectroscopy). Transmission electron microscopy (TEM) observations were performed by using JEOL JEM2010 microscope at acceleration voltage of 200 kV. The areal mass density (*amd*), of network was calculated by using ImageJ computer program (NIH, Bethesda, MD, USA) using "Ridge detection" plugin. The *amd* corresponds to the silver mass per unit area (usually expressed in mg/m^2). The *amd* mentioned is the average taken from 5 SEM images. The structural properties were investigated by X-ray diffraction analysis (XRD, BRUKER D8 ADVANCE). The measurements were carried out through a 2Θ scan range from 6° to 100°, using Bragg-Brentano

configuration and Cu Kα (0.1541 nm) radiation. The thermal stability of the TE was monitored by performing temperature ramps using a hot plate in air, with 5 °C/min of heating rate. The resistance was measured using a Keithley 2400 instrument (Keithley Instruments Inc., Cleveland, OH, USA) with 2-probe system at a voltage of 0.1 V. Raman measurements were performed with a Jobin Yvon Horiba Olympus BX41 at room temperature and using a green laser (514 nm).

The electrochemical measurements of V_2O_5 coated films were carried out in a three-electrode cell using a BioLogic VSP potentiostat/galvanostat, equipped with the EC-Lab software. A platinum foil was used as counter electrode, while a saturated calomel electrode (SCE, Hg / Hg_2Cl_2 / saturated aqueous solution of KCl, E_{SCE} = 0.234 V/NHE) was used as reference electrode. The measurements were carried out between -0.5 V and +0.9 V with a scan rate of 20 mV/s. Chronoamperometry measurements were also recorded by applying -0.5 V for reduction and +0.9 V for oxidation, with a pulse duration of 60 s. *In situ* optical measurements were carried out at 400 nm during the chronoamperometry test. The baseline for optical measurement was taken with glass tank and electrolyte. The switching time was calculated from the transmittance curve corresponding to oxidation and reduction *versus* time. The coloration efficiency was quantified by evaluating the change in optical density *versus* charge density.

3. RESULTS AND DISCUSSION

3.1 Study of the bare silver nanowire (AgNW) network as transparent electrode

The morphology of typical AgNW networks deposited by spray deposition is shown in the SEM image in Figure 1a, where the random nature of the AgNW network is clearly seen. The optical and electrical properties of AgNW-based TE mainly depend on the *amd* of the AgNW network. Figure 1b shows the dependence of the optical transparency, haziness and sheet resistance (R_{sh}) of the AgNW networks *versus amd*. The total transmittance, for instance at 550 nm, decreases linearly

with increasing *amd*, from 69 to 126 mg/m^2. Such dependency can be simply explained by shadowing effects[48]. The optical transmittance of AgNW having *amd* of 69, 88, and 126 mg/m^2 is 80, 74, and 66 % at 550 nm (with substrate reflection/absorption), respectively. R_{sh} also decreases when *amd* increases, following a power law[48]. AgNW networks having *amd* of 88 mg/m^2 were used for the further study. Similar data for a bare ITO film is also reported in Figure 1b, for the sake of comparison.

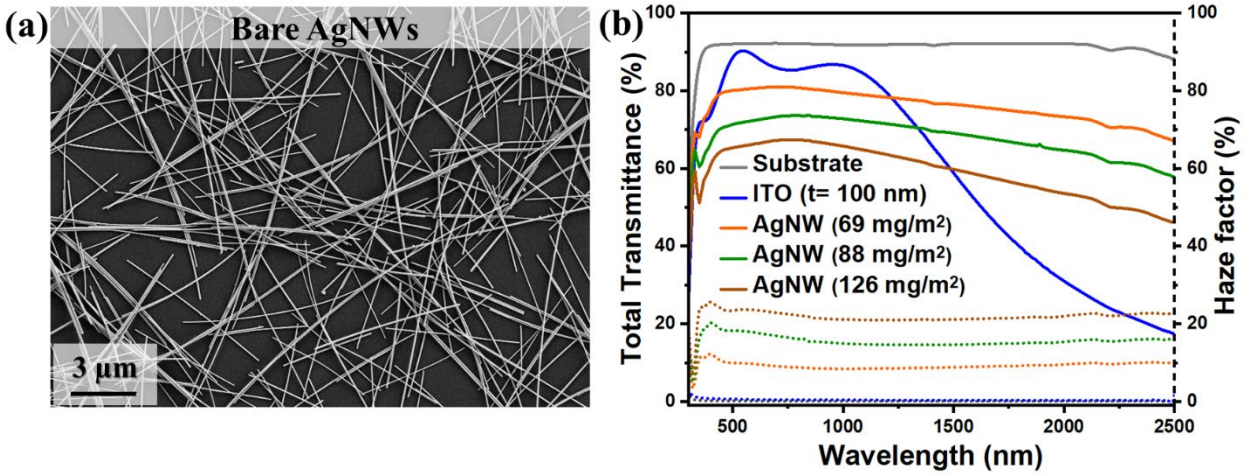

Figure 1. (a) Scanning electron microscopy (SEM) observation of AgNW network with *amd* value of 88 mg/m², (b) effect of various *amd* values on the optical (total transmittance and haze factor shown in left and right axis, respectively) and electrical properties (sheet resistance) of AgNW network. The associated sheet resistance values for AgNW networks are respectively 10, 5 and 2 Ω/sq for the *amd* values of 69, 88 and 126 mg/m², while the sheet resistance for ITO thin film is 16 Ω/sq.

The AgNW network is responsible for the electrical conductivity whereas the spaces between AgNWs are responsible for the optical transparency. Therefore, in agreement with Figure 1b, larger *amd* leads to an increase of surface coverage, reducing optical transparency and lowering sheet resistance thanks to a larger number of electrical paths within the network. Moreover, the

haze factor, which is the ratio of diffuse transmittance to the total transmittance, increases with the *amd* values due to the light-scattering effect of the nanowires in the visible range. The higher haze factor significantly diminishes the visual quality of optically transparent films. A possible solution is to incorporate smaller nanowire diameters and/or an increase in nanowire length, which may aid in mitigating the haze factor without compromising electrical properties[49-50].

AgNW network were obtained through simple overlapping of nanowires during the spray deposition. This resulted in a rather weak contact at the junctions between AgNWs and therefore the contact resistance between them can exhibit rather high values. The junctions of the AgNW network can be optimized thanks to a mild annealing. Based on the previous work from our group[21], the AgNW networks were subjected to 200 °C for 1 h in air.

3.2 Study of the coated silver nanowire (AgNW) networks as transparent electrode

The stability of AgNWs is important to avoid the degradation in the deposition conditions used for electrochromic oxide layer. In order to improve the stability of AgNW networks, they were coated with 20 nm and 30 nm thin coatings of protective oxides (either SnO_2 or ZnO) using different number of AP-SALD cycles[38]. The morphologies of bare and coated AgNWs are shown in the SEM images in Figure 2a-c, and the TEM image of a single AgNW shown in the inset. The coated AgNW with 30 nm thick ZnO and SnO_2 are presented in Figure 2b-c. The TEM image of SnO_2 coated film (in the inset) shows a very conformal coating. The thickness of protective oxide coating (ZnO or SnO_2) observed through TEM analysis is confirmed to be 30 nm. The SEM and TEM images of 20 nm thick coated oxides layer can be found in Figure S2a-b. This is worth noticing that the interface between AgNW and the metal oxide coating appears without significant defects, which constitutes a requirement for a AgNW network stability improvement.

Figure 2d represents the thermal ramp of both a bare and a coated AgNW network, providing valuable insights into the thermal stability by monitoring the TE resistance with increasing temperature. The normalized resistance (measured resistance divided by the initial resistance) *versus* temperature is plotted. The variation in the morphology at the junction of the AgNWs networks before and after thermal treatment was investigated using SEM, and the corresponding images are reported in Figure 2d inset.

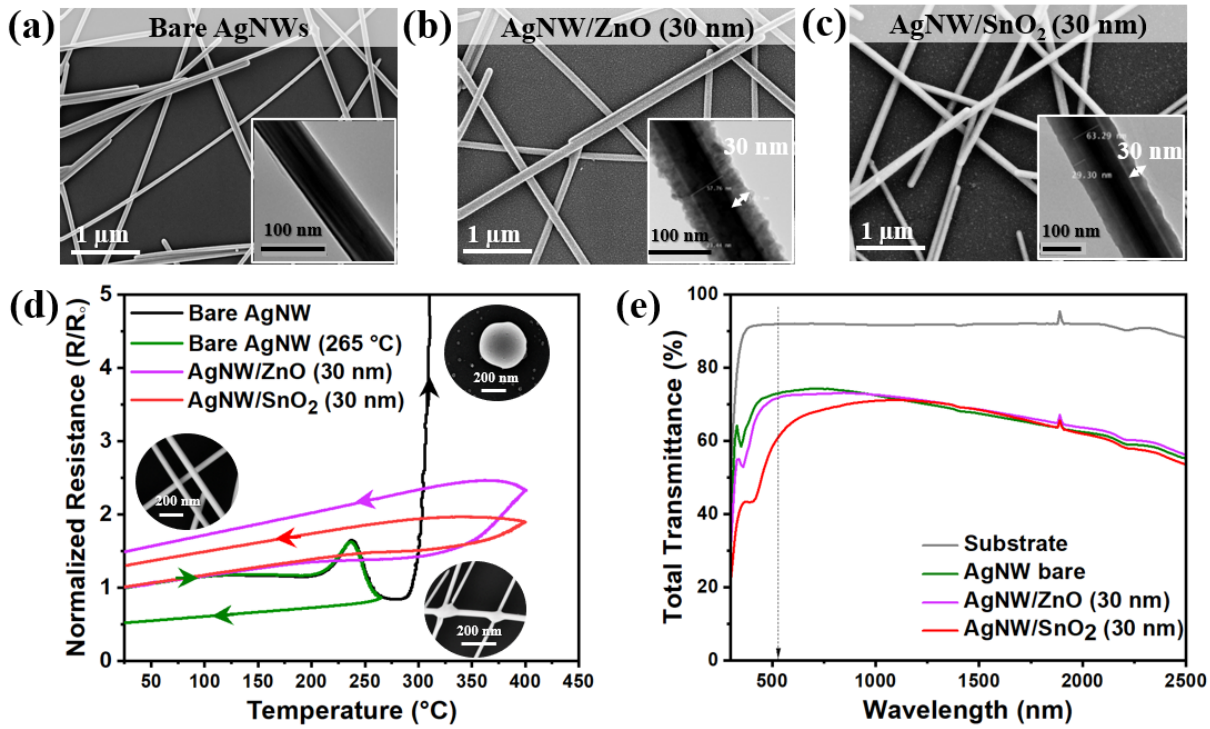

Figure 2. Scanning electron microscopy (SEM) and transmission electron microscopy (TEM, in inset) (a) observations of bare AgNW, (b) 30 nm thick ZnO-coated AgNWs, and (c) 30 nm thick SnO_2-coated AgNWs. (d) Normalized electrical resistance (resistance divided by its initial value R_0) *versus* temperature during a thermal ramp in air at 5 °C/min from room temperature to 400 °C, for bare AgNWs (black curve), ZnO coated AgNWs (magenta curve) and SnO_2 coated AgNWs (red curve). Additionally, a thermal ramp from room temperature to 265 °C was performed on bare AgNWs (green curve). The insets show the SEM images of bare AgNWs before thermal ramp,

sintering effect after a thermal ramp up to 265 °C and spheroidization after a thermal ramp up to 400 °C. (e) Optical transmittance spectra of glass substrate, bare and coated AgNW network with 30 nm thick of either ZnO or SnO_2 layers.

The temperature up to 150 °C with small increase in resistance corresponds to electron-phonon interaction. This linear increase in resistance with temperature is due to metallic behavior of AgNW networks[21]. In this region, the AgNW network junctions remain poorly connected like untreated nanowires as shown in the SEM image (Figure 2d inset). For temperature between 200 to 240 °C, the resistance increase represents moderate degradation of weak junctions of AgNW network (probably those which exhibit the smaller AgNW diameter and the associated junctions). This is followed by a decrease in resistance up to temperature of 270 °C, this can be interpreted as local sintering of junctions which improved the conductivity of AgNW network. This was validated by a thermal ramp up to 265 °C on another bare AgNW sample at the same rate and cooled down back to room temperature (green curve in Figure 2d). The resistance dropped to half from initial value due to improved contact at the junctions. SEM images also demonstrate the sintering of junction that took place thanks to atomic silver diffusion[21], (see Figure 2d inset). A noticeable degradation is observed for bare AgNWs, upon heating above 300 °C. This degradation is confirmed by a significant increase in resistance, indicating a decline in the electrical conductivity of the bare AgNW network. Consequently, the thermal stability of bare AgNWs is compromised under higher temperature conditions. At high temperature thermal energy activates the diffusion of silver atoms and the nanowires become spheroidized, forming Ag droplets, and the network lose its percolative nature, as shown in the SEM image in Figure 2d inset. The driving force associated to such morphology change is the surface energy reduction, such phenomenon is called Plateau-Rayleigh instability[21]. In contrast, the coated AgNWs exhibited remarkable stability

even at 400 °C. The resistance of ZnO coated AgNW increased from 4.7 to 7 Ω after the thermal ramp. However, for SnO_2 coated AgNWs the resistance increases solely to 5.9 Ω, which is not a significant increase. As expected, the oxide coatings improved the thermal stability of AgNW network, furthermore SnO_2 appears more stable than ZnO[38].

The optical transmittance shows a decrease in transmittance after the oxide coating of 30 nm thickness as shown in Figure 2e. The decrease for ZnO is only a 1.1 %, whereas for SnO_2 coated sample it is approximately a 11 %, at 550 nm wavelength. There is a trade-off between the transparency and durability of AgNW network, the trade-off being piloted by the oxide layer thickness. An increase of the oxide layer thickness improves the stability of the AgNWs, but this often comes at the cost of reduced transparency. Such a trade-off depends on the specific requirements of the targeted application.

3.3 Structure and morphology of electrochromic V_2O_5 thin films deposited on coated AgNW network

Figure 3 shows the XRD patterns of the different thin films before and after V_2O_5 deposition. The peaks around 38.1° and 44.7° on the XRD patterns of bare AgNWs, ZnO coated (30 nm) and SnO_2 coated (30 nm) AgNWs can be indexed as (111) and (200) planes for FCC Pmmn silver (JCPDS card file no. 04–0783). An additional peak at 32.2° visible for bare AgNW can be attributed to the (111) plane of cubic Ag_2O (JCPDS 41-1104) that could be present on the surface of AgNWs[49, 51]. The silver oxide decomposes below 200 °C[52], therefore the peak disappeared after the protective oxide coating deposited at 200 °C. The XRD patterns for AgNW/ZnO (30 nm) and AgNW/SnO_2 (30 nm) do not show any extra peaks corresponding to ZnO or SnO_2 since the protective oxide layer is quite thin. However, grazing angle XRD recorded at an incidence angle of 2.0° for AgNW/ZnO (30 nm) reveals distinct peaks at 2θ angles of 31.8°, 34.4°, 36.3°, and 56.8°

as shown in Figure S3a. These peaks correspond to the crystallographic planes (100), (002), (101), and (110) of hexagonal ZnO phase, corresponding to JCPDS Card No.00-005-0664, respectively[53]. However, SnO_2 coated AgNW networks only exhibit the XRD peaks associated to AgNWs since SnO_2-coating is amorphous (Figure S3b) at the temperature used for deposition (200 °C)[41].

The diffractogram of V_2O_5 layer deposited on bare-AgNWs clearly illustrates the disappearance of peaks associated to AgNW as shown in Figure 3. On the contrary, the oxide coated (30 nm thick) films show XRD peaks for both silver and V_2O_5. The peak observed at a diffraction angle of 20.2° can be attributed to the (001) plane of orthorhombic V_2O_5 with the Pmmn space group (JCPDS No 089-2482). The presence of crystalline silver confirms that AgNW network with 30 nm thick oxide coating are stable in sputtering conditions. On contrary, AgNWs coated either with 20 nm thick ZnO or SnO_2 are not stable in the sputtering conditions, resulting in disappearance of crystalline silver peak, as shown in Figure S4. This degradation of AgNWs is further proved by Raman, SEM, and EDS mapping results.

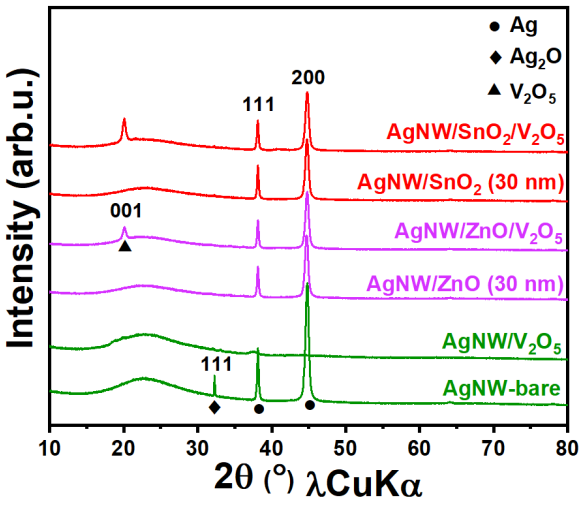

Figure 3. X-Ray diffraction patterns of bare AgNW network, and coated AgNWs (with 30 nm thick ZnO or SnO_2 coating) before and after V_2O_5 deposition.

The Raman spectra of the bare AgNWs, and V_2O_5 films are presented in Figure S5. The peak at 240 cm^{-1} for the bare-AgNW corresponds to the Ag-O stretching vibration mode due to the presence of Ag_2O which is also observed in XRD of bare AgNW[54-55]. The 30 nm thick ZnO or SnO_2 coated AgNWs exhibit distinct characteristic Raman peaks that correspond to crystalline orthorhombic V_2O_5. The peaks observed at 105 cm^{-1}, 148 cm^{-1}, and 196 cm^{-1} are associated to the bending vibration of O-V-O bonds within VO_5 square pyramids. The low frequency peaks reveal the presence of long range ordered vanadium-oxygen layer modes[56]. The peaks at 285 cm^{-1} and 405 cm^{-1}, are associated to V=O bending vibrations and at 484 cm^{-1} is assigned to the V-O-V bending vibration. The Raman peaks at high frequency are associated to the V-O stretching vibrations. Peaks at 530 cm^{-1} and 704 cm^{-1} are ascribed to triply coordinated and doubly coordinated O-V stretching modes of vibration, respectively. The peak at 997 cm^{-1} is assigned to V=O (vanadyl mode) stretching vibration[57]. These findings align well with the XRD results.

The morphology of V_2O_5 deposited on bare and coated AgNWs are shown in Figure 4a-c. The bare AgNWs become highly resistive after V_2O_5 deposition due to the lack of an efficient protective layer and result in the disappearance of network shape as depicted from Figure 4a, and Table 1. The latter summarizes the prevailing features before and after the V_2O_5 coating. These results are in close agreement with XRD analysis.

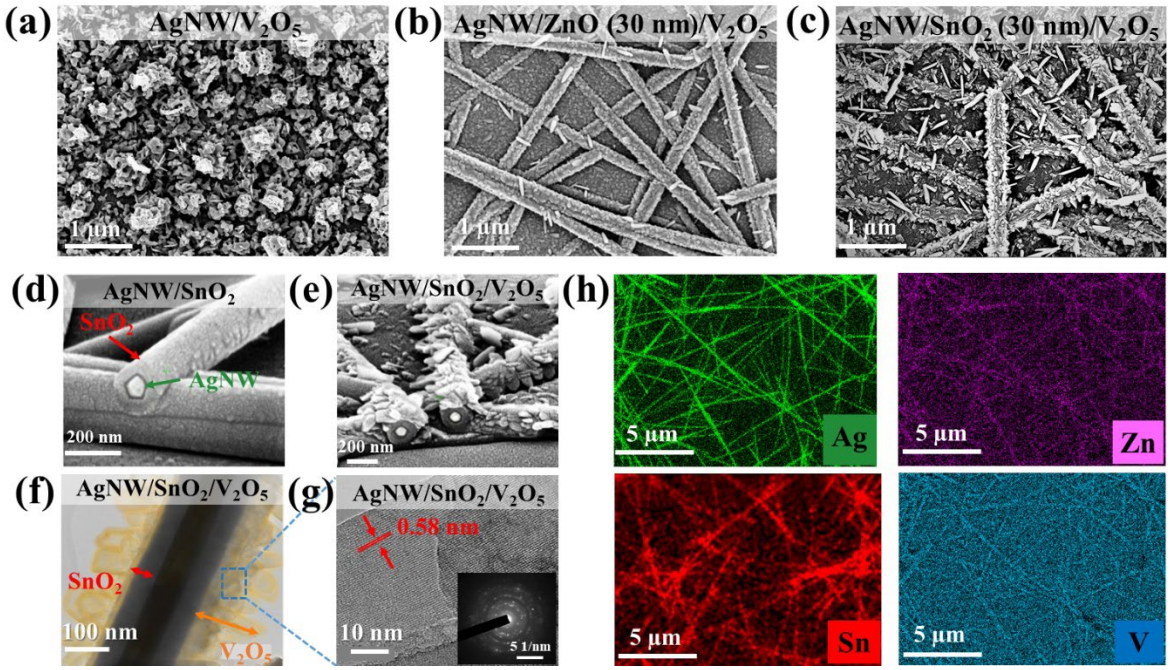

Figure 4. SEM images of bare and 30 nm thick oxide-coated AgNW network after V_2O_5 deposition. a) V_2O_5 on bare-AgNWs, (b) V_2O_5 on ZnO-coated AgNWs, (c) V_2O_5 on SnO_2-coated AgNWs, (d-e) Cross-section SEM images of SnO_2 coated AgNW before and after V_2O_5, respectively, (f) TEM image of SnO_2 coated AgNW after V_2O_5 coating, (g) SAED pattern of V_2O_5 on coated AgNWs, (h) EDS elemental mapping of silver for AgNW, zinc for ZnO coating, tin from SnO_2 coating, and vanadium from V_2O_5 for AgNW/SnO_2 (30 nm)/V_2O_5.

The coated AgNWs show uniform distribution of V_2O_5 flakes grown on the surface of AgNWs and glass substrate (Figure 4b-c). The cross-section of AgNW with SnO_2 coating shows a pentagonal shape of AgNW covered by a conformal layer of oxide (Figure 4d). The cross-section SEM image of V_2O_5 film indicates the presence of five-fold AgNW symmetry surrounded by SnO_2 coating and the flakes of V_2O_5. In case of bare and 20 nm thick oxide coated AgNWs the degradation of AgNW is visible after the electrochromic V_2O_5 oxide sputtering (Figure S6a-c). The stability of the thin 20 nm layer of oxide coating appears rather low to sustain the AgNWs

network during V_2O_5 sputtering deposition. The appearance of flake like structure represents the growth of V_2O_5 on the AgNW network. These results are in good agreement with XRD data, corresponding to a successful growth of V_2O_5 films on stable 30 nm SnO_2 coated AgNWs. The length of the V_2O_5 flakes ranges between 100 -150 nm and the width is around 50 nm, as deduced from TEM observation (Figure 4f). The lattice fringes corresponding to V_2O_5 and exhibit a regular spacing of 0.58 nm, which corresponds to the interplanar distance of (200) plane of V_2O_5 (Figure 4g). The well-resolved fringes and SAED pattern confirm the crystallinity of V_2O_5 as observed by XRD as well.

The EDS mapping of Ag, Zn, Sn, and V collected from AgNW/SnO_2 (30 nm)/V_2O_5 are reported in Figure 4h. It shows the presence of silver as a randomly oriented AgNW network. Zinc and tin from protective oxides coatings are distributed uniformly on the AgNW network as well as on the glass substrate for both AgNW/ZnO (30 nm)/V_2O_5 and AgNW/SnO_2 (30 nm)/V_2O_5. Similarly, vanadium can also be seen on the entire AgNWs surface as well as on the substrate. However, in case of 20 nm thick oxide coated samples, AgNW network is degraded and silver is distributed over the whole substrate (Figure S6d-g). This is the result of degradation of coating layer both ZnO and SnO_2 which fail to protect silver atomic diffusion and degrading of AgNWs during the sputtering step.

Table 1. Prevailing features of AgNW network before and after V_2O_5 coating

AgNW	**Resistance before V_2O_5 deposition (Ω)**	**Resistance after V_2O_5 deposition (Ω)**	**AgNW Network**
Bare	16	Highly resistive	Degraded
ZnO (20 nm)	10	Highly resistive	
SnO_2 (20 nm)	10	8.10^5	
ZnO (30 nm)	10	15	Non-degraded

SnO_2 (30 nm)	10	15	

In order to evaluate the sputtering conditions responsible for the degradation of bare and ZnO coated AgNWs, during sputtering, the stability test has been performed. Bare AgNWs and 20 nm thick ZnO coated AgNWs were annealed at 210 °C for 80 min in the sputtering chamber in the presence of argon only, as observed for deposition of V_2O_5. The samples were then characterized by XRD, 2-probe resistance measurement and SEM analysis before and after Ar annealing. The resistance of both samples remained unchanged following the annealing and no degradation in morphology was observed (Figure S7a-b). Moreover, XRD peaks of silver remained consistent for both samples after annealing (Figure S7c). This represents that the disappearance of AgNW network is not due to temperature evolution but it could be due to presence of reactive plasma in the deposition chamber.

3.4 Electrochromic performance

Electrochromic performance of the deposited films with 30 nm thick protective oxide coating was determined through cyclic voltammetry and chronoamperometry. The cyclic voltammogram of AgNW-bare/V_2O_5, AgNW/ZnO/V_2O_5 and AgNW/SnO_2/V_2O_5 are shown in Figure 5a. The CV curve of bare and ZnO-coated samples neither show any oxidation and reduction peak nor the change in color. Similar behavior is observed by V_2O_5 films having 20 nm thick oxide coated AgNW (Figure S8). The potential was applied between -0.5 V and +0.9 V *versus* SCE, at 20 mV/s sweep rate. AgNW network coated with 30 nm thick ZnO was stable in sputtering condition but not in the electrolyte at the applied potential. This could be due to the dissolution of ZnO layer since the electrolyte can reach the ZnO layer due to flaky nature of V_2O_5. On the contrary, 30 nm SnO_2-coated AgNW sample shows the distinguished anodic and cathodic peaks characteristics of V_2O_5[58], showing the better stability enhancement of SnO_2 compared to ZnO. Upon CV cycling,

lithium ion progressively intercalated into the structure, yielding $Li_xV_2O_5$, in which the reduction from V^{5+} to V^{4+} has taken place. The color of the film changes from orange to blue. The CV shows two cathodic peaks observed at +0.3 V and +0.06 V. The reduction is limited to -0.5 V where the current density is almost constant. The reaction is completely reversible with the appearance of two corresponding anodic peaks at +0.3 V and +0.5 V, when the potential is reversed to +0.9 V. This corresponds to the deintercalation of Li^+ from the $Li_xV_2O_5$ accompanied by a reversible change in color back to orange. The intercalation and deintercalation of Li^+ are shown by the following reaction 1:

$$V_2O_{5\,(Orange)} + xLi^+ + xe^- \leftrightarrow Li_xV_2O_{5(blue)} \qquad (1)$$

The electrochemical capacity Q (C/cm²) involved in the redox reaction is calculated from $\int j.\,dV/v$, the integrated area associated to J-V curve where j is current density, V is potential and v is the sweep rate (equal to 20 mV/s). The electrochemical capacity of SnO_2-coated AgNW-V_2O_5 sample is 37.9 mC/cm^2 for Li^+ intercalation and 37.3 mC/cm^2 for Li^+ deintercalation. The stability of the electrochromic layer, on SnO_2 coated AgNW, was tested and demonstrated by performing 500 CV cycles, all of which presented the same shape (Figure 5b). This indicates the good reversibility of the film. Moreover, the AgNWs and V_2O_5 remain crystalline after 500 cycles, which is in good agreement with XRD observations reported in Figure S9.

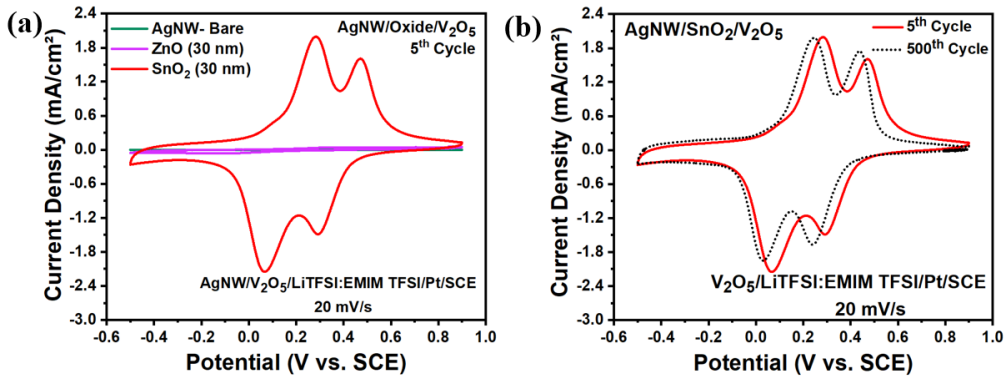

Figure 5. (a) Cyclic voltammetry curves of V_2O_5 samples on bare-AgNWs and coated AgNWs with ZnO or SnO_2 for an applied potential between -0.5 V and +0.9 V with a sweep rate of 20 mV/s, (b) Cycling stability of AgNW/SnO_2 (30 nm)/V_2O_5 showing 5th and 500th cycles.

The switching time is a relevant characteristic of electrochromic films and refers to the time necessary to observe a 90 % change in optical contrast from the initial value. The switching time of V_2O_5 sample was deduced from *in situ* transmittance spectra recorded at the wavelength of 400 nm during a chronoamperogram (CA). The CA associated to AgNW/SnO_2/V_2O_5 film is obtained by applying the reduction potential of -0.5 V for a duration of 60 seconds as shown in Figure 6a. The current density is recorded at regular intervals of 0.1 s. The potential is then switched to +0.9 V for another 60 s, and the corresponding current density is measured again. The switching time corresponded to 6.0 s in oxidation and 8.6 s in reduction as shown in Figure 6a.

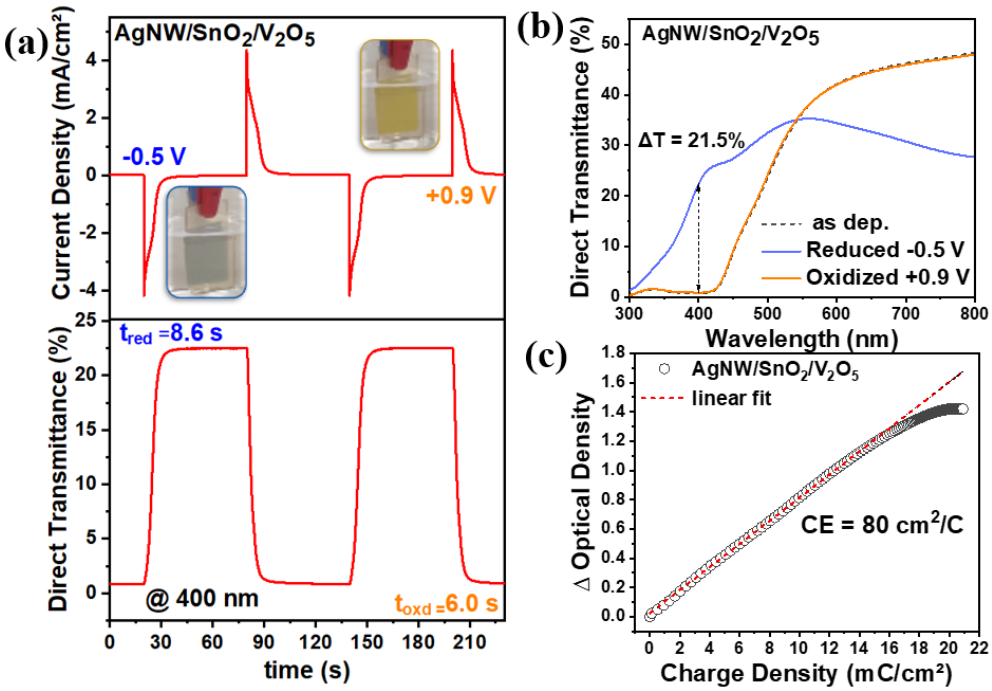

Figure 6. *In situ* opto-electrochemical measurements of AgNW/SnO_2 (30 nm)/V_2O_5 film (a) Chronoamperogram (top) at -0.5 V for reduction and +0.9 V for oxidation for 60 s each and switching time (bottom) under the application of the same voltage (-0.5 V, +0.9 V). The inset images show colors of a film in oxidized and reduced states. (b) Optical transmittance in the as-deposited, oxidized and reduced state of the V_2O_5, showing optical contrast at a wavelength of 400 nm. (c) Variation of optical density *versus* the charge density, which enables to deduce the coloration efficiency at 400 nm.

The electrochromic performance of the V_2O_5 film was also evaluated from optical transmission modulation or optical contrast (ΔT%), and coloration efficiency (CE(λ)). The optical contrast is estimated by using Eq. 2:

$$\Delta T\%_{(400\ nm)} = T_{reduced}\ (\%) - T_{oxidized}\ (\%) \qquad (2)$$

Where, $T_{(reduced)}$ represents transmittance of film in Li^+ intercalated state and $T_{(oxidized)}$ represents transmittance in Li^+ de-intercalated state. The optical transmittance of the film in as-deposited state, reduced (Li^+ intercalated) and oxidized (Li^+ de-intercalated) state was measured from 300 to 800 nm wavelength. The transmittance of the film in as deposited state and oxidized state is identical, as shown in Figure 6b, indicating a good coloration reversibility. The optical contrast of the film, calculated by using Eq. 2 is found to be 21.5 % at 400 nm. The coloration efficiency (CE) is the criteria of merit for electrochromic materials. The CE of the film is estimated from Eq. 3:

$$CE(\lambda) = \frac{\Delta OD(\lambda)}{Q} \qquad (3)$$

where, λ denotes the wavelength, Q is the charge density (calculated from charge deinsertion per unit area) and $\Delta OD_{(\lambda)}$ is the change in optical density given by:

$$\Delta OD(\lambda) = \log\left(\frac{Treduced(\%)}{Toxidized(\%)}\right) \qquad (4)$$

The coloration efficiency of the V_2O_5 film at wavelength 400 nm is found to be 80 cm^2/C. Panagopoulou et al. recorded coloration efficiency of 84.5 cm^2/C at 400 nm on RF sputtered V_2O_5 films using ITO based TE[59]. Lin et al. prepared V_2O_5 film on ITO TE, that exhibits a coloration efficiency of 102 cm^2/C at 400 nm[60]. The electrochromic results on AgNW based TE films are therefore comparable to the previously reported results on ITO based films. The higher CE indicates that a large optical contrast can be obtained by a small charge intercalation or de-intercalation. To the best of our knowledge, this work presents the first-time successful sputtering of V_2O_5 films on coated AgNW networks used as the transparent electrode.

CONCLUSIONS

Aiming at cost efficient electrochromic systems, the replacement of ITO layer by AgNWs network as TE was investigated. The stability of AgNWs was achieved by the deposition of a conformal protecting oxide coating of ZnO or SnO_2 using SALD. The deposition of V_2O_5 thin films, on bare AgNWs, ZnO-coated and SnO_2-coated AgNW with thicknesses of 20 or 30 nm, by RF magnetron sputtering technique leads to orange V_2O_5 film. However, AgNWs network coated with only 30 nm thick oxide layer results to crystallized V_2O_5, while fruitless growth associated with degradation of the AgNWs network for bare AgNWs and 20 nm thick oxide coated is reported. The V_2O_5 film on 30 nm thick SnO_2 coated AgNWs shows nice electrochemical switching in between orange to blue with a stability of at least 500 cycles in lithium-based electrolyte. This study is a step forward in the development of electrochromic devices, both in the visible and near infrared regions, free of ITO, that are highly desirable in particular in respect of scarcity, cost, flexibility and suitability, opening up multiple application fields.

ASSOCIATED CONTENT

Supporting Information. The supporting information is available free of charge

Temperature evolution monitored every 10 min during 80 min of V_2O_5 sputtering on AgNW samples (Figure S1), SEM observations of 20 nm thick oxide-coated AgNW network (a) ZnO-coated AgNWs (b) SnO_2-coated AgNWs (Figure S2), grazing incidence diffraction (GIXRD) with an incidence angle of 2.0° for (a) AgNW/ZnO and (b) AgNW/SnO_2 samples (Figure S3), XRD pattern of coated AgNW (with 20 nm thick ZnO or SnO_2 coating) network before and after V_2O_5 layer deposition (Figure S4), Raman spectra of bare AgNW and V_2O_5 films of 30 nm thick coated AgNWs (Figure S5), SEM images of 20 nm thick coated AgNW network after V_2O_5 deposition of (a) bare-AgNWs (b) V_2O_5 on ZnO-coated AgNWs (c) V_2O_5 on SnO_2-coated AgNWs, EDS elemental mapping of (d) degraded AgNW, (e) tin for 20 nm SnO_2 coated sample (f) zinc for 20 nm ZnO coating, and (g) vanadium for V_2O_5 coating (Figure S6), the stability of bare-AgNWs and ZnO-coated AgNWs after annealing at 210 °C temperature for 80 min in the sputtering chamber at 2 Pa pressure in Ar atmosphere, without plasma. SEM image after annealing in Ar atmosphere of (a) bare-AgNW (b) 20 nm thick ZnO coated AgNW (c) XRD of bare-AgNW and AgNW/ZnO (20 nm) after annealing (Figure S7), cyclic voltammetry curves of V_2O_5 on bare, ZnO (20 nm thick) coated AgNW and SnO_2 (20 nm thick) coated AgNW samples for an applied potential between -0.5 V and +0.9 V at a sweep rate of 20 mV/s (Figure S1), XRD data obtained before and after 500 CV cycles on AgNW/SnO_2 (30 nm)/V_2O_5 sample (Figure S2)

AUTHOR INFORMATION

Corresponding Author

Daniel Bellet: Daniel.bellet@grenoble-inp.fr

Aline Rougier: Aline.rougier@icmcb.cnrs.fr

Author Contributions

Conceptualization, A.K., A.R. and D.B.; AgNW deposition, A.K., L.B. and C.S.-V.; AgNW characterization, A.K., L.B. and C. J.; SALD oxide deposition, C.S.-V. and D. M.-R.; Sputtering deposition and V_2O_5 characterization, A.K., B.F., S.S. N. and A.R.; Electrochemical analysis: A.A., B.F., S.S. N. and A.R.; writing—original draft preparation, A.K., A.R. and D.B.; writing—review and editing, all authors; supervision, A.R. and D.B.; project administration, C.J.; funding acquisition, A.R. and D.B. All authors have read and agreed to the published version of the manuscript.

Funding Sources

This work was funded by the project M-Era-Net INSTEAD (2021-2024).

ACKNOWLEDGMENT

We warmly thank Laetitia Rapenne for the TEM analysis and Hervé Roussel for the XRD analysis. Thanks to the thin film facilities and in particular Lionel Teulé-Gay for technical assistance and fruitful discussions. Eric Lebraud is thanked for his help on GIXRD measurements. Brandon Faceira thanks the University of Bordeaux for funding his Ph.D. grant.

REFERENCES

1. Pérez-Lombard, L.; Ortiz, J.; Pout, C. A Review on Buildings Energy Consumption Information. *Energy Build.* **2008,** *40*, 394-398.

2. Tavares, P. F.; Gaspar, A. R.; Martins, A. G.; Frontini, F. Evaluation of Electrochromic Windows Impact in the Energy Performance of Buildings in Mediterranean Climates. *Energy Policy* **2014,** *67*, 68-81.

3. Granqvist, C. G. Electrochromics for Smart Windows: Oxide-Based Thin Films and Devices. *Thin solid films* **2014,** *564*, 1-38.

4. Karaca, G. Y.; Eren, E.; Cogal, G. C.; Uygun, E.; Oksuz, L.; Oksuz, A. U. Enhanced Electrochromic Characteristics Induced by Au/PEDOT/Pt Microtubes in WO_3 Based Electrochromic Devices. *Opt. Mater* **2019,** *88*, 472-478.

5. Gies, M.; Rempel, T.; Becker, M.; Polity, A. Advantageous Optical Characteristics of Tantalum Vanadium Oxide as Counter Electrode in Electrochromic Devices. *J. Mater. Sci.* **2022,** *57*, 12810-12823.

6. Ellmer, K. Past Achievements and Future Challenges in the Development of Optically Transparent Electrodes. *Nat. Photonics* **2012,** *6*, 809-817.

7. Ahmad, K.; Shinde, M. A.; Song, G.; Kim, H. Design and Fabrication of $Mose_2/Wo_3$ Thin Films for the Construction of Electrochromic Devices on Indium Tin Oxide Based Glass and Flexible Substrates. *Ceram. Int.* **2021,** *47*, 34297-34306.

8. Shinde, M. A.; Kim, H. Highly Stable Silver Nanowire-Based Transparent Conductive Electrodes for Electrochromic Devices. *Mater. Today Commun.* **2021,** *26*, 102147.

9. Hecht, D. S.; Hu, L.; Irvin, G. Emerging Transparent Electrodes Based on Thin Films of Carbon Nanotubes, Graphene, and Metallic Nanostructures. *Adv. Mater.* **2011,** *23*, 1482-1513.

10. Paul, S.; Kim, D.-W. Preparation and Characterization of Highly Conductive Transparent Films with Single-Walled Carbon Nanotubes for Flexible Display Applications. *Carbon* **2009,** *47*, 2436-2441.

11. Peng, K.; Liu, L.-Q.; Gao, Y.; Qu, M.-Z.; Zhang, Z. Fabrication of High Optical Transparent and Conductive Swnt Based Transparent Conducting Film on Flexible Plastic Substrate Using Ozone as a Redox Dopant. *J. Nanosci. Nanotechnol.* **2010,** *10*, 7386-7389.

12. Bae, S.; Kim, S. J.; Shin, D.; Ahn, J.-H.; Hong, B. H. Towards Industrial Applications of Graphene Electrodes. *Phys. Scr.* **2012,** *2012*, 014024.

13. Wang, P.; Jian, M.; Zhang, C.; Wu, M.; Ling, X.; Zhang, J.; Wei, B.; Yang, L. Highly Stable Graphene-Based Flexible Hybrid Transparent Conductive Electrodes for Organic Solar Cells. *Adv. Mater. Interfaces* **2022,** *9*, 2101442.

14. Cai, G.; Darmawan, P.; Cui, M.; Wang, J.; Chen, J.; Magdassi, S.; Lee, P. S. Highly Stable Transparent Conductive Silver Grid/PEDOT: PSS Electrodes for Integrated Bifunctional Flexible Electrochromic Supercapacitors. *Adv. Energy Mater.* **2016,** *6*, 1501882.

15. Sharma, M.; Pudasaini, P. R.; Ruiz-Zepeda, F.; Elam, D.; Ayon, A. A. Ultrathin, Flexible Organic–Inorganic Hybrid Solar Cells Based on Silicon Nanowires and Pedot: Pss. *ACS Appl. Mater. Interfaces* **2014,** *6*, 4356-4363.

16. Yin, Y.; Lan, C.; Guo, H.; Li, C. Reactive Sputter Deposition of Wo3/Ag/Wo3 Film for Indium Tin Oxide (Ito)-Free Electrochromic Devices. *ACS Appl. Mater. Interfaces* **2016,** *8*, 3861-3867.

17. De, S.; Higgins, T. M.; Lyons, P. E.; Doherty, E. M.; Nirmalraj, P. N.; Blau, W. J.; Boland, J. J.; Coleman, J. N. Silver Nanowire Networks as Flexible, Transparent, Conducting Films: Extremely High Dc to Optical Conductivity Ratios. *ACS Nano* **2009,** *3*, 1767-1774.

18. Lagrange, M.; Langley, D.; Giusti, G.; Jiménez, C.; Bréchet, Y.; Bellet, D. Optimization of Silver Nanowire-Based Transparent Electrodes: Effects of Density, Size and Thermal Annealing. *Nanoscale* **2015,** *7*, 17410-17423.

19. Papanastasiou, D. T.; Schultheiss, A.; Muñoz-Rojas, D.; Celle, C.; Carella, A.; Simonato, J. P.; Bellet, D. Transparent Heaters: A Review. *Adv. Funct. Mater.* **2020,** *30*, 1910225.

20. Sannicolo, T.; Lagrange, M.; Cabos, A.; Celle, C.; Simonato, J. P.; Bellet, D. Metallic Nanowire-Based Transparent Electrodes for Next Generation Flexible Devices: A Review. *Small* **2016,** *12*, 6052-6075.

21. Langley, D.; Lagrange, M.; Giusti, G.; Jiménez, C.; Bréchet, Y.; Nguyen, N. D.; Bellet, D. Metallic Nanowire Networks: Effects of Thermal Annealing on Electrical Resistance. *Nanoscale* **2014,** *6*, 13535-13543.

22. Mayousse, C.; Celle, C.; Fraczkiewicz, A.; Simonato, J.-P. Stability of Silver Nanowire Based Electrodes under Environmental and Electrical Stresses. *Nanoscale* **2015,** *7*, 2107-2115.

23. Khaligh, H. H.; Xu, L.; Khosropour, A.; Madeira, A.; Romano, M.; Pradére, C.; Tréguer-Delapierre, M.; Servant, L.; Pope, M. A.; Goldthorpe, I. A. The Joule Heating Problem in Silver Nanowire Transparent Electrodes. *Nanotechnology* **2017,** *28*, 425703.

24. Patil, J. J.; Chae, W. H.; Trebach, A.; Carter, K. J.; Lee, E.; Sannicolo, T.; Grossman, J. C. Failing Forward: Stability of Transparent Electrodes Based on Metal Nanowire Networks. *Adv. Mater.* **2021,** *33*, 2004356.

25. Chen, D.; Liang, J.; Liu, C.; Saldanha, G.; Zhao, F.; Tong, K.; Liu, J.; Pei, Q. Thermally Stable Silver Nanowire–Polyimide Transparent Electrode Based on Atomic Layer Deposition of Zinc Oxide on Silver Nanowires. *Adv. Funct. Mater.* **2015,** *25*, 7512-7520.

26. Zhang, B.; Liu, D.; Liang, Y.; Zhang, D.; Yan, H.; Zhang, Y. Flexible Transparent and Conductive Films of Reduced-Graphene-Oxide Wrapped Silver Nanowires. *Mater. Lett.* **2017,** *201*, 50-53.

27. Kholmanov, I. N.; Stoller, M. D.; Edgeworth, J.; Lee, W. H.; Li, H.; Lee, J.; Barnhart, C.; Potts, J. R.; Piner, R.; Akinwande, D. Nanostructured Hybrid Transparent Conductive Films with Antibacterial Properties. *ACS Nano* **2012,** *6*, 5157-5163.

28. Wu, C.; Jiu, J.; Araki, T.; Koga, H.; Sekitani, T.; Wang, H.; Suganuma, K. Rapid Self-Assembly of Ultrathin Graphene Oxide Film and Application to Silver Nanowire Flexible Transparent Electrodes. *RSC Adv.* **2016,** *6*, 15838-15845.

29. Aliprandi, A.; Moreira, T.; Anichini, C.; Stoeckel, M. A.; Eredia, M.; Sassi, U.; Bruna, M.; Pinheiro, C.; Laia, C. A.; Bonacchi, S. Hybrid Copper-Nanowire–Reduced-Graphene-Oxide Coatings: A “Green Solution” toward Highly Transparent, Highly Conductive, and Flexible Electrodes for (Opto) Electronics. *Adv. Mater.* **2017,** *29*, 1703225.

30. Hao, T.; Wang, S.; Xu, H.; Zhang, X.; Magdassi, S.; Pan, L.; Song, Y.; Li, Y.; Zhao, J. Novel Transparent TiO_2/Agnw–Si (NH_2)/PET Hybrid Films for Flexible Smart Windows. *ACS Appl. Mater. Interfaces* **2022,** *14*, 21613-21622.

31. Ahn, Y.; Jeong, Y.; Lee, Y. Improved Thermal Oxidation Stability of Solution-Processable Silver Nanowire Transparent Electrode by Reduced Graphene Oxide. *ACS Appl. Mater. Interfaces* **2012,** *4*, 6410-6414.

32. Chae, W. H.; Sannicolo, T.; Grossman, J. C. Double-Sided Graphene Oxide Encapsulated Silver Nanowire Transparent Electrode with Improved Chemical and Electrical Stability. *ACS Appl. Mater. Interfaces* **2020,** *12*, 17909-17920.

33. Song, T.-B.; Rim, Y. S.; Liu, F.; Bob, B.; Ye, S.; Hsieh, Y.-T.; Yang, Y. Highly Robust Silver Nanowire Network for Transparent Electrode. *ACS Appl. Mater. Interfaces* **2015,** *7*, 24601-24607.

34. Aghazadehchors, S.; Nguyen, V. H.; Munoz-Rojas, D.; Jiménez, C.; Rapenne, L.; Nguyen, N. D.; Bellet, D. Versatility of Bilayer Metal Oxide Coatings on Silver Nanowire Networks for Enhanced Stability with Minimal Transparency Loss. *Nanoscale* **2019,** *11*, 19969-19979.

35. Wang, L.; Huang, D.; Li, M.; Xu, H.; Zou, J.; Tao, H.; Peng, J.; Xu, M. Highly Transparent and Thermal-Stable Silver Nanowire Conductive Film Covered with Znmgo by Atomic-Layer-Deposition. *J. Phys. Chem. Solids* **2017,** *111*, 328-334.

36. Muñoz-Rojas, D.; Nguyen, V. H.; de La Huerta, C. M.; Aghazadehchors, S.; Jiménez, C.; Bellet, D. Spatial Atomic Layer Deposition (SALD), an Emerging Tool for Energy Materials. Application to New-Generation Photovoltaic Devices and Transparent Conductive Materials. *C. R. Phys.* **2017,** *18*, 391-400.

37. Khan, A.; Nguyen, V. H.; Muñoz-Rojas, D.; Aghazadehchors, S.; Jiménez, C.; Nguyen, N. D.; Bellet, D. Stability Enhancement of Silver Nanowire Networks with Conformal Zno Coatings

Deposited by Atmospheric Pressure Spatial Atomic Layer Deposition. *ACS Appl. Mater. Interfaces* **2018,** *10*, 19208-19217.

38. Bardet, L.; Papanastasiou, D. T.; Crivello, C.; Akbari, M.; Resende, J.; Sekkat, A.; Sanchez-Velasquez, C.; Rapenne, L.; Jiménez, C.; Muñoz-Rojas, D. Silver Nanowire Networks: Ways to Enhance Their Physical Properties and Stability. *Nanomaterials* **2021,** *11*, 2785.

39. Nguyen, V. H.; Resende, J.; Papanastasiou, D. T.; Fontanals, N.; Jiménez, C.; Muñoz-Rojas, D.; Bellet, D. Low-Cost Fabrication of Flexible Transparent Electrodes Based on Al Doped Zno and Silver Nanowire Nanocomposites: Impact of the Network Density. *Nanoscale* **2019,** *11*, 12097-12107.

40. Bardet, L.; Akbari, M.; Crivello, C.; Rapenne, L.; Weber, M.; Nguyen, V. H.; Jiménez, C.; Muñoz-Rojas, D.; Denneulin, A.; Bellet, D. SnO_2-Coated Silver Nanowire Networks as a Physical Model Describing Their Reversible Domain under Electrical Stress for Stable Transparent Electrode Applications. *ACS Appl. Nano Mater.* **2023,** *6*, 15234–15246.

41. Nguyen, V. H.; Akbari, M.; Sekkat, A.; Ta, H. T.; Resende, J.; Jiménez, C.; Musselman, K. P.; Muñoz-Rojas, D. Atmospheric Atomic Layer Deposition of Sno_2 Thin Films with Tin (II) Acetylacetonate and Water. *Dalton Trans.* **2022,** *51*, 9278-9290.

42. Mortimer, R. J. Electrochromic Materials. *Annu. Rev. Mater. Res.* **2011,** *41*, 241-268.

43. Le, T. K.; Pham, P. V.; Dong, C.-L.; Bahlawane, N.; Vernardou, D.; Mjejri, I.; Rougier, A.; Kim, S. W. Recent Advances in Vanadium Pentoxide (V_2O_5) Towards Related Applications in Chromogenics and Beyond: Fundamentals, Progress, and Perspectives. *J. Mater. Chem. C* **2022,** *10*, 4019-4071.

44. Mjejri, I.; Rougier, A.; Gaudon, M. Low-Cost and Facile Synthesis of the Vanadium Oxides V_2O_3, VO_2, and V_2O_5 and Their Magnetic, Thermochromic and Electrochromic Properties. *Inorg. Chem.* **2017,** *56*, 1734-1741.

45. Mjejri, I.; Gaudon, M.; Song, G.; Labrugère, C.; Rougier, A. Crystallized V_2o_5 as Oxidized Phase for Unexpected Multicolor Electrochromism in V_2O_5 Thick Film. *ACS Appl. Energy Mater.* **2018,** *1*, 2721-2729.

46. Zhang, W.; Li, H.; Al-Hussein, M.; Elezzabi, A. Y. Electrochromic Battery Displays with Energy Retrieval Functions Using Solution-Processable Colloidal Vanadium Oxide Nanoparticles. *Adv. Opt. Mater.* **2020,** *8*, 1901224.

47. Nguyen, V. H.; Resende, J.; Jiménez, C.; Deschanvres, J.-L.; Carroy, P.; Munoz, D.; Bellet, D.; Muñoz-Rojas, D. Deposition of Zno Based Thin Films by Atmospheric Pressure Spatial Atomic Layer Deposition for Application in Solar Cells. *J. Renew. Sustain. Energy* **2017,** *9*, 021203.

48. Bellet, D.; Lagrange, M.; Sannicolo, T.; Aghazadehchors, S.; Nguyen, V. H.; Langley, D. P.; Muñoz-Rojas, D.; Jiménez, C.; Bréchet, Y.; Nguyen, N. D. Transparent Electrodes Based on Silver Nanowire Networks: From Physical Considerations Towards Device Integration. *Materials* **2017,** *10*, 570.

49. Wang, T.; Xiao, H.; Gao, Y.; Xu, J.; Zhang, Z.; Bian, H.; Sun, T. Ag_2O/TiO_2 Hollow Microsphere Heterostructures with Exposed High-Energy {001} Crystal Facets and High Photocatalytic Activities. *J. Mater. Sci.: Mater. Electron.* **2020,** *31*, 11496-11507.

50. Araki, T.; Jiu, J.; Nogi, M.; Koga, H.; Nagao, S.; Sugahara, T.; Suganuma, K. Low Haze Transparent Electrodes and Highly Conducting Air Dried Films with Ultra-Long Silver Nanowires Synthesized by One-Step Polyol Method. *Nano Research* **2014,** *7*, 236-245.

51. Yang, H.; Ren, Y.-y.; Wang, T.; Wang, C. Preparation and Antibacterial Activities of $Ag/Ag^{+}/Ag^{3+}$ Nanoparticle Composites Made by Pomegranate (Punica Granatum) Rind Extract. *Results Phys.* **2016,** *6*, 299-304.

52. Chiu, Y.; Rambabu, U.; Hsu, M.-H.; Shieh, H.-P. D.; Chen, C.-Y.; Lin, H.-H. Fabrication and Nonlinear Optical Properties of Nanoparticle Silver Oxide Films. *J. Appl. Phys.* **2003,** *94*, 1996-2001.

53. Fatah, S. K. Synthesis and Characterisation of Zinc Oxide Nanopowders Prepared by Precipitation Method. *Diyala J. Pure Sci.* **2018,** *14*, 40-47.

54. Giesz, P.; Mackiewicz, E.; Nejman, A.; Celichowski, G.; Cieślak, M. Investigation on Functionalization of Cotton and Viscose Fabrics with Agnws. *Cellulose* **2017,** *24*, 409-422.

55. Martina, I.; Wiesinger, R.; Jembrih-Simbürger, D.; Schreiner, M. Micro-Raman Characterisation of Silver Corrosion Products: Instrumental Set up and Reference Database. *E-Preserv. Sci.* **2012,** *9*, 1-8.

56. Julien, C.; Nazri, G.; Bergström, O. Raman Scattering Studies of Microcrystalline V_6O_{13}. *Phys. Status Solidi B* **1997,** *201*, 319-326.

57. Koduru, H. K.; Obili, H. M.; Cecilia, G. Spectroscopic and Electrochromic Properties of Activated Reactive Evaporated Nano-Crystalline V_2O_5 Thin Films Grown on Flexible Substrates. *Int. Nano Lett.* **2013,** *3*, 1-8.

58. Avellaneda, C. O. Electrochromic Performance of Sol–Gel Deposited V_2O_5: Ta Films. *Mater. Sci. Eng. B* **2007,** *138*, 118-122.

59. Panagopoulou, M.; Vernardou, D.; Koudoumas, E.; Tsoukalas, D.; Raptis, Y. S. Oxygen and Temperature Effects on the Electrochemical and Electrochromic Properties of Rf-Sputtered V_2o_5 Thin Films. *Electrochim. Acta* **2017,** *232*, 54-63.

60. Lin, Y.-S.; Tsai, C.-W.; Chen, P.-W. Electrochromic Properties of V_2O_5− Z Thin Films Sputtered onto Flexible PET/ITO Substrates. *Solid State Ion.* **2008,** *179*, 290-297.

For Table of Contents Only